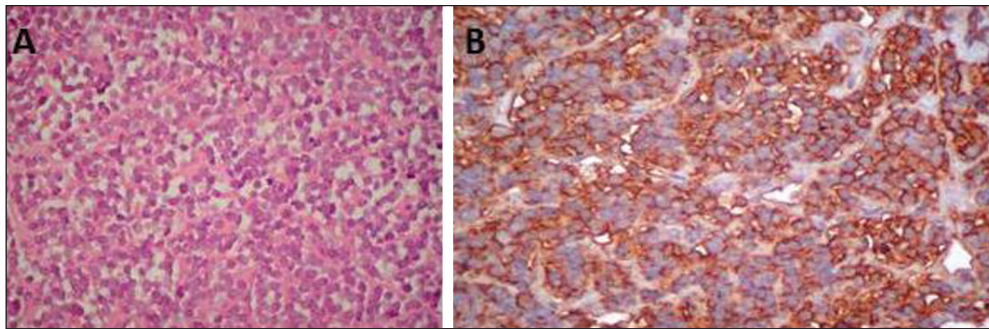


**Figure 1. A:** Axial T2-weighted MRI scan showing a huge heterogeneous retroperitoneal mass (green arrow) with an isointense intradural component (red arrow). **B:** Axial gadolinium contrast-enhanced T1-weighted image showing a large mass, with intense peripheral enhancement and central necrosis (red arrow), extending through the neural foramen (yellow arrow).



**Figure 2. A:** Hematoxylin-eosin staining (original magnification,  $\times 40$ ) showing dense cellular proliferation in a diffuse or vaguely lobular pattern of uniform round cells, with scanty cytoplasm, ovoid nuclei with fine chromatin and small nucleoli. Note also the delicate fibrous vascular stroma. **B:** CD99 (MIC-2) staining showing strong immunoreactivity of the cytoplasmic membrane.

The majority of ES/ETs are diagnosed during the first two decades of life<sup>(1)</sup>. The most common soft tissue sites are the chest wall, lower extremities, and pelvis/hip region. They are rarely found in the retroperitoneum, upper extremities, or internal organs<sup>(2)</sup>. Patients often present with a painless mass or vague abdominal or chest pain, depending on tumor site<sup>(1)</sup>. Muscle weakness can also be the predominant symptom<sup>(3)</sup>.

There are certain red flags that should always be considered in the differential diagnosis of patients with focal neurological manifestations of myelopathy and radiculopathy. Although rare and having no specific radiological findings, ES/ET should be suspected in young adults presenting with a large heterogeneous mass in the trunk, extremities, or soft tissues<sup>(4)</sup>. In the case presented here, an MRI finding of a large mass with isointense solid components on T1- and T2-weighted images, together with necrosis and hemorrhage, facilitated the diagnosis in this intriguing case. In addition, ES of the retroperitoneum is difficult to differentiate from other tumors. The retroperitoneal tumors that can invade the neural foramen and vertebral canal are the following: ganglioneuroma and ganglioneuroblastoma; neuroblastoma in younger patients (mean age, 22 months); leukemia (chloroma); and lymphoma. Invasion of the renal vein, inferior vena cava, and liver can be seen in ES, renal cell carcinoma, and adrenocortical carcinoma. Differentiation aspects that favor the diagnosis of ES are earlier age of presentation, absence of metastatic lymphadenopathy, and absence of calcifications. ES

tends to be unilateral and does not cross midline<sup>(5)</sup>. The definitive diagnosis can be made only by histopathological analysis.

**REFERENCES**

1. Javery O, Krajewski K, O'Regan K, et al. A to Z of extraskeletal Ewing sarcoma family of tumors in adults: imaging features of primary disease, metastatic patterns, and treatment responses. *AJR Am J Roentgenol.* 2011;197:W1015–22.
2. Ma Z, Brimo F, Zeizafoun N. Primary Ewing's sarcoma/primitive neuroectodermal tumor (ES/PNET) of the penis: a report of an extraordinarily unusual site and a literature review of extraskeletal Ewing's sarcoma. *Int J Surg Pathol.* 2013;21:63–7.
3. Sade R, Çakir M, Oğul H, et al. Primary extraosseous Ewing sarcoma of the lumbar spine presenting with left leg weakness. *Spine J.* 2015;15: 1488–9.
4. Holland MT, Flouty OE, Close LN, et al. A unique case of primary Ewing's sarcoma of the cervical spine in a 53-year-old male: a case report and review of the literature. *Case Rep Med.* 2015;2015:402313.
5. Somarouthu BS, Shinagare AB, Rosenthal MH, et al. Multimodality imaging features, metastatic pattern and clinical outcome in adult extraskeletal Ewing sarcoma: experience in 26 patients. *Br J Radiol.* 2014; 87:20140123.

**Fabiano Reis<sup>1</sup>, Eduardo Macedo<sup>1</sup>, Marcondes Cavalcanti França Junior<sup>1</sup>, Eliane Ingrid Amstalden<sup>1</sup>, Simone Appenzeller<sup>1</sup>**

1. Universidade Estadual de Campinas (Unicamp), Campinas, SP, Brazil. Mailing address: Dr. Fabiano Reis. Unicamp – Radiologia. Rua Tessália Vieira de Camargo, 126, Cidade Universitária. Campinas, SP, Brazil, 13083-887. E-mail: fabianoreis2@gmail.com.

<http://dx.doi.org/10.1590/0100-3984.2015.0236>

**Ultrasound evaluation of diaphragmatic dysfunction**

Dear Editor,

A 49-year-old male patient presented with a complaint of dyspnea when swimming, which he did regularly. The following were performed: chest X-ray, which showed elevation of the right hemidiaphragm; respiratory function tests, which revealed mild restrictive lung disease; and ultrasound of the diaphragm, which

demonstrated a significant reduction in the mobility of the right hemidiaphragm, although not to the point of paralysis.

Ultrasound of the diaphragm has been used mainly in patients in intensive care. In such patients, assessment of the diaphragm by ultrasound can be used in order to predict successful weaning from mechanical ventilation<sup>(1)</sup>, to inform decisions regarding adjustments in mechanical ventilation parameters, and to investigate postoperative weakness/diaphragmatic paralysis<sup>(2)</sup>,

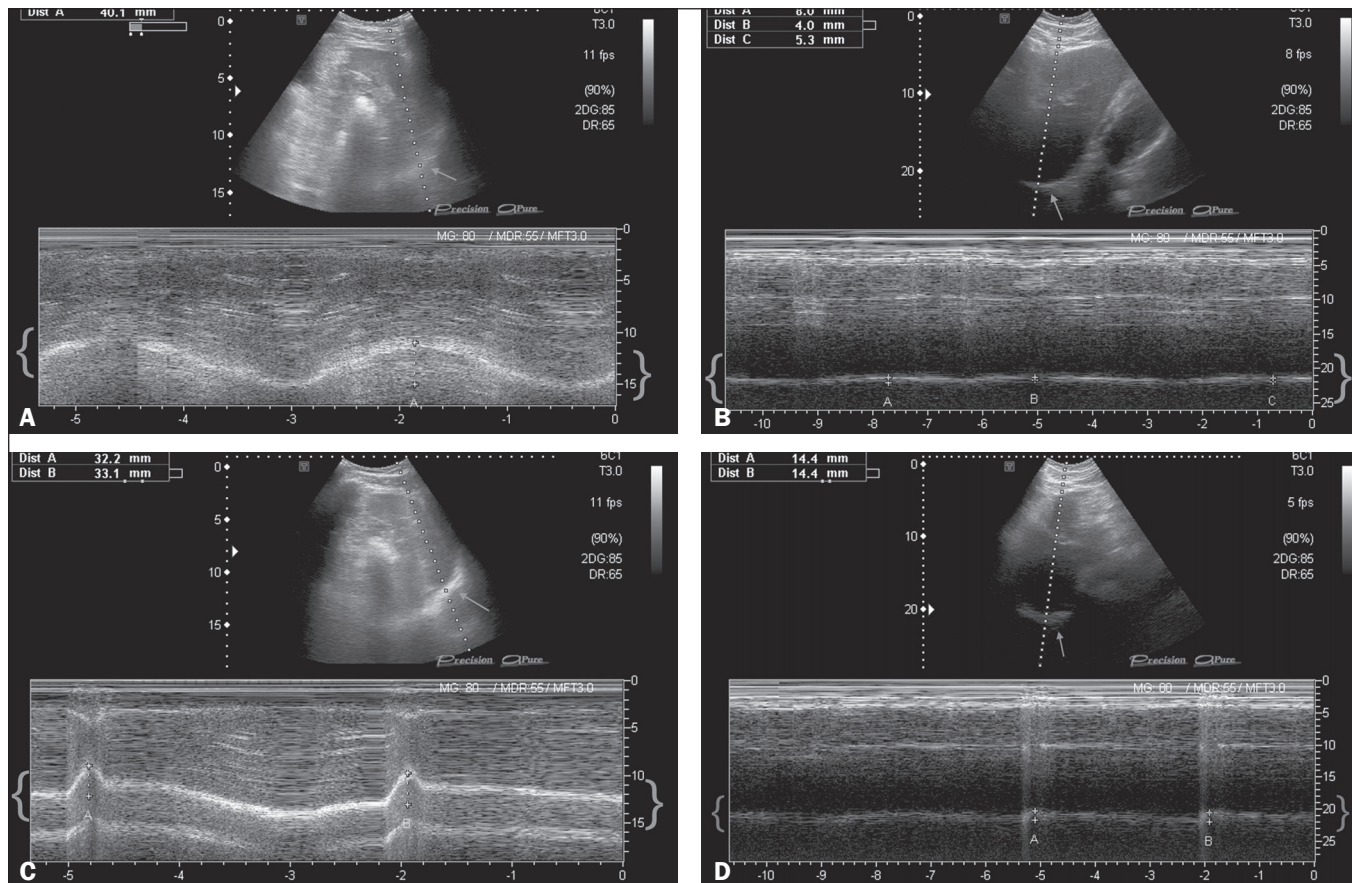


**Figure 1. A:** M-mode ultrasound during quiet breathing. Left hemidiaphragm. The curve between braces represents the normal trajectory of diaphragm mobility during quiet breathing. The arrow shows the left hemidiaphragm, accessed via the anterior subcostal route, in the oblique plane with a spleen window, in B mode. **B:** M-mode ultrasound during quiet breathing. Right hemidiaphragm. The curve between braces shows that there was a major reduction in the mobility of the right hemidiaphragm. The arrow shows the right hemidiaphragm, accessed via the subcostal route, with a liver window, in B mode. **C:** M-mode ultrasound during sniffing. Left hemidiaphragm. The curve between braces represents the normal trajectory of diaphragm mobility during sniffing. The arrow shows the left hemidiaphragm, accessed via the anterior subcostal route, in the oblique plane with a spleen window, in B mode. **D:** M-mode ultrasound during sniffing. Right hemidiaphragm. The curve between braces shows that there was a major reduction in the mobility of the right hemidiaphragm during sniffing. The arrow shows the right hemidiaphragm, accessed via the subcostal route, with a liver window, in B mode.

as well as to identify diaphragmatic atrophy after prolonged mechanical ventilation<sup>(3)</sup>. In the present report, two radiologists evaluated the thickness and mobility of the diaphragm, using B-mode and M-mode ultrasound, respectively. The evaluations were made by consensus.

In the B-mode evaluation, the hemidiaphragms were accessed via the intercostal spaces. With the patient in the supine position, a linear multifrequency (7–18 MHz) transducer was positioned in the longitudinal plane on the anterior axillary line, between the 7th and 8th or 8th and 9th intercostal spaces<sup>(4)</sup>. Assessments were made at the zone of apposition, where the diaphragm abuts the lower rib cage<sup>(5)</sup>. The normal diaphragm was visualized between two echogenic lines<sup>(1)</sup>: that of the parietal pleura and that of the peritoneal membrane. Three measurements of muscle thickness were performed during maximal inspiration and expiration maneuvers, and the unweighted mean was calculated for each maneuver. During inspiration, there was contraction and shortening of the fibers of the normal diaphragm, with increased muscle volume and consequent thickness. We calculated the diaphragm thickening fraction (DTF, defined as  $\text{inspiratory thickness} - \text{expiratory thickness} / \text{expiratory thickness} \times 100\%$ ), which quantifies the degree of muscle thickening from functional residual capacity to total lung capacity, using the mean of the measurements<sup>(5)</sup>.

In the M-mode evaluation, the right hemidiaphragm was accessed via the anterior subcostal route, obliquely between the hemiclavicular and anterior axillary lines, and the left hemidiaphragm was accessed via the intercostal route, on the middle axillary line. In either case, the patient was placed in the supine position and a convex 2-5 MHz transducer was used<sup>(4)</sup>. Curves of the diaphragm kinetics were acquired under three respiratory conditions<sup>(2)</sup>: quiet breathing, deep breathing, and sniffing. In each condition, we obtained three waves and their respective amplitudes, calculating the unweighted mean of the measurements.

The maximum inspiratory and expiratory thickness of the diaphragm was 0.29 cm and 0.22 cm, respectively, for the right hemidiaphragm, compared with 0.35 cm and 0.20 cm, respectively, for the left hemidiaphragm. The DTF was 31% and 73% for the right and left hemidiaphragms, respectively. In the quiet breathing, deep breathing, and sniffing conditions, the mobility of the diaphragm was 0.57 cm, 2.24 cm, and 1.24 cm, respectively, for the right hemidiaphragm, compared with 4.53 cm and 3.44 cm for the left hemidiaphragm in the quiet breathing and sniffing conditions, respectively (Figure 1). It was not possible to determine the mobility of the left hemidiaphragm during deep breathing, probably due to the small size of the (spleen) window.

In the case reported here, the mobility of the right hemidiaphragm was significantly reduced. However, we did not identify

diaphragmatic paralysis, the diagnostic criteria for which are a DTF below 20% in B-mode<sup>(5)</sup> and paradoxical breathing, characterized by a curve below the baseline in M-mode<sup>(6)</sup>. At this writing, the patient is being monitored and is under conservative treatment, showing gradual clinical improvement.

REFERENCES

1. Ferrari G, De Filippi G, Elia F, et al. Diaphragm ultrasound as a new index of discontinuation from mechanical ventilation. *Crit Ultrasound J.* 2014;6:8.
2. Matamis D, Soilemezi E, Tsagourias M, et al. Sonographic evaluation of the diaphragm in critically ill patients. Technique and clinical applications. *Intensive Care Med.* 2013;39:801–10.
3. Francis CA, Hoffer JA, Reynolds S. Ultrasonographic evaluation of diaphragm thickness during mechanical ventilation in intensive care patient. *Am J Crit Care.* 2016;25:e1–8.

4. Sarwal A, Walker FO, Cartwright MS. Neuromuscular ultrasound for evaluation of the diaphragm. *Muscle Nerve.* 2013;47:319–29.
5. Summerhill EM, El-Sameed YA, Glidden TJ, et al. Monitoring recovery from diaphragm paralysis with ultrasound. *Chest.* 2008;133:737–43.
6. Lloyd T, Tang YM, Benson MD, et al. Diaphragmatic paralysis: the use of M mode ultrasound for diagnosis in adults. *Spinal Cord.* 2006;44:505–8.

Rachel Zeitoune<sup>1</sup>, Ana Célia Baptista Koifman<sup>2</sup>, Marina Shu Fong<sup>1</sup>, Roberto Mogami<sup>1</sup>

1. Hospital Universitário Pedro Ernesto (HUPE), Rio de Janeiro, RJ, Brazil. 2. Hospital Universitário Gaffrée & Guinle (HUGG), Rio de Janeiro, RJ, Brazil. Mailing address: Dra. Rachel Zeitoune. Hospital Universitário Pedro Ernesto – Serviço de Radiologia. Boulevard 28 de Setembro, 77, Vila Isabel. Rio de Janeiro, RJ, Brazil, 20551-030. E-mail: raczei@hotmail.com.

<http://dx.doi.org/10.1590/0100-3984.2016.0072>

**Malignant peripheral nerve sheath tumor of the vagus nerve: an uncommon cause of progressive dyspnea**

Dear Editor,

A healthy, nonsmoking, 27-year-old male patient was referred to our institution for investigation of a three-month history of progressive dyspnea. He reported that his dyspnea worsened on physical exertion and significantly limited his daily activities. He reported no cough, fever, night sweats, or weight loss; nor did he report any new lumps or masses during the last three months. Upon skin examination, multiple subcutaneous nodules and *café-au-lait* spots were noted, together with bilateral axillary freckles (Figure 1a). Collectively, those clinical findings met the criteria for a diagnosis of neurofibromatosis, which was so far undiagnosed. Pulmonary auscultation revealed diffuse wheezing in the right upper hemithorax. His biochemical profile was unremarkable. The patient then underwent a

computed tomography (CT) scan of the chest with intravenous contrast administration, which revealed a 20-cm right cervicothoracic mass presumably arising from the right vagus nerve (Figures 1b–d). Because of the background of neurofibromatosis, a hypothesis of malignant peripheral nerve sheath tumor (MPNST) was raised and further confirmed by incisional biopsy and histological analysis. Given the proximity to vital structures, the patient was treated with a chemotherapy protocol for soft tissue sarcomas in an attempt to reduce the tumor bulk preoperatively. Because of a poor cellular response and recrudescence of the respiratory symptoms, the patient was deemed ineligible for any aggressive interventions.

MPNSTs are exceedingly rare sarcomas in the general population, with a lifetime risk of less than 0.01%. Conversely, in association with neurofibromatosis, these tumors arise in higher frequency because of malignant transformation from preexisting plexiform neurofibromas<sup>(1)</sup>. Overall, these tumors are associated

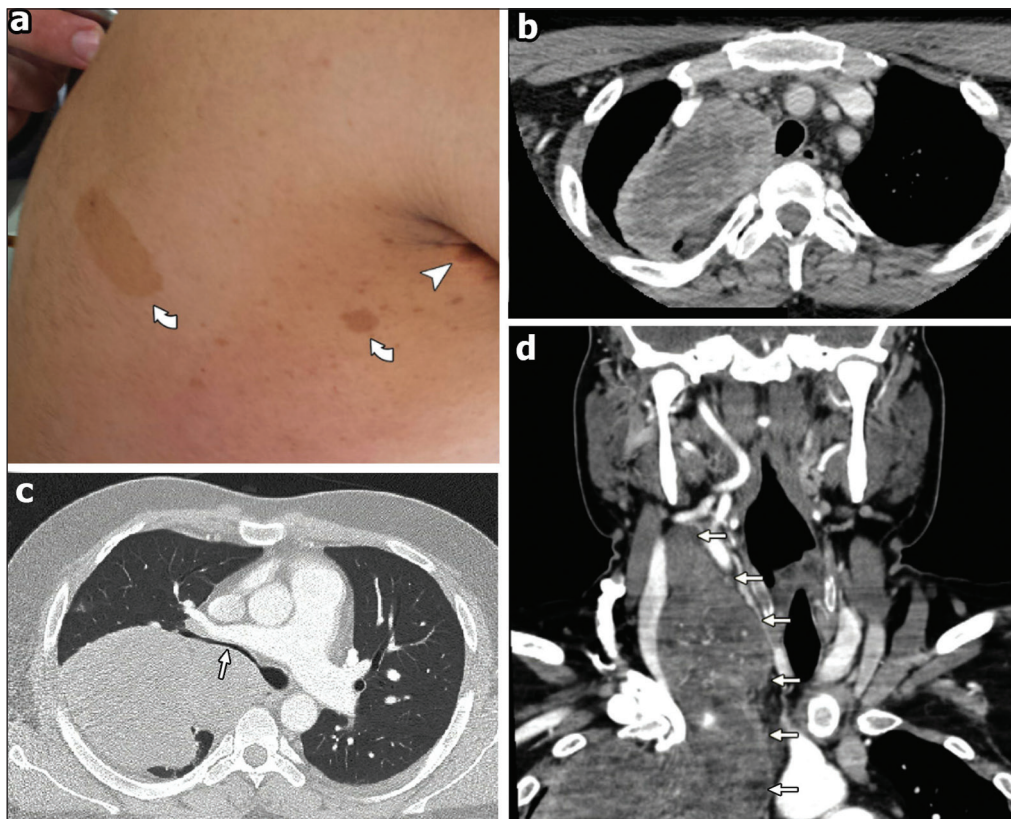


**Figure 1.** Findings on physical examination and CT. **a:** *Café-au-lait* spots (curved arrows) and axillary freckles (arrowhead) upon skin inspection. **b–d:** Axial CT scans of the neck (**b,d**) and chest (**c,d**) showing the MPNST. Note the heterogeneous enhancement after contrast administration (**b**) and the stenosis of the right main bronchus lumen (**c**), which accounts for the auscultation findings.